Thermo-mechanical fatigue damage behavior for Ni-based superalloy under multiaxial loading

Dao-Hang Li and *De-Guang* Shang*

College of Mechanical Engineering and Applied Electronics Technology, Beijing University of Technology, 100124 Beijing, China

Abstract. The fatigue damage behavior was experimentally investigated in different axial-torsional thermo-mechanical loading conditions for Ni-based superalloy GH4169. The strain controlled tests were carried out with the same von Mises equivalent mechanical strain amplitude of 0.8% in the temperature range from 360°C to 650°C. The results show that the fatigue life is drastically reduced when the axial mechanical strain and the temperature are in-phase, which can be due to that the creep damage is induced by the tensile stress at high temperature. Moreover, the fatigue life is further decreased when the axial mechanical strain and the shear strain are out-of-phase, which can be attributed to that the non-proportional hardening can increase the creep and the oxidation damages. Furthermore, the tensile stress is crucial to the nucleation of creep cavities at high temperature compared with the shear stress. The tensile and shear stresses all can increase the creep damage under fatigue loading at high temperature. In addition, the oxidation damage can be induced during cyclic loading at high temperature, and it can be increased by the tensile mean stress caused in non-isothermal loading.

1 Introduction

In recent years the fatigue behavior of material under thermo-mechanical loading has become the focus of investigation, in which various damage mechanisms are existed simultaneously. For improving the accuracy of life prediction, the involved damage mechanisms during thermo-mechanical fatigue (TMF) loading need to be identified.

Many investigations [1-12] have assessed the fatigue damage behavior of material under uniaxial TMF loading. The results show that the thermal phase angle (between the axial mechanical strain waveform and the temperature waveform) has an important influence on fatigue life. For some superalloys [1-5], the fatigue life under in-phase (IP) TMF loading is obviously lower than that under out-of-phase (OP) TMF loading. During the IP TMF loading, the creep damage is caused besides the fatigue damage, which leads to the intergranular fracture of material, and this fracture mode can be the main reason of drastic decrease in fatigue life. For the OP TMF loading, the fatigue damage is dominant [1], in which the transgranular fracture is the primary failure mode. Moreover, for the above superalloys, the oxidation damage is also caused [6, 8], but it cannot play a dominant role. For some other superalloys [9-12], the OP TMF loading induces more serious damage compared with the IP TMF loading. The oxidation damage is dominant under OP TMF loading for these superalloys, and the high tensile stress corresponding low temperature can increase the oxidation damage. In common, the above investigations show that the damage mechanism is quite complex during TMF loading, and it is varied with the different loading conditions and materials. In addition, it is noteworthy that in the vast majority of the above investigations the tested thermal phase angle is only at 0° and 180°, thus the fatigue damage behavior under TMF loading in other thermal phase angle case needs to be further assessed.

Furthermore, the fatigue damage behavior under multiaxial TMF loading has been assessed in some investigations [13-18]. Axial-torsional thermo-mechanical fatigue (AT-TMF) tests can be used to understand some special fatigue behavior in non-isothermal multiaxial loading condition, in which the mechanical phase angle (between the axial mechanical strain waveform and the shear strain waveform) also needs to be controlled. So the effect of mechanical phase angle on fatigue damage behavior under AT-TMF loading has become a new investigation focus.

In addition, since the Ni-based superalloy has fine mechanical properties, corrosion resistance, good weld ability and long-term thermal stability [19], it is widely used in the structural components of modern gas turbine engines subjected to multiaxial thermo-mechanical fatigue loading. Thus the Ni-based superalloy is chosen to understand the fatigue damage behavior under AT-TMF loading.

In this paper, the main aim is to analyze the existed various damage mechanisms under AT-TMF loading. Moreover, the effects of thermal and mechanical phase angles on fatigue damage behavior and the influences of involved fatigue, creep and oxidation damages on fatigue life under AT-TMF loading will be discussed in detail.

* Corresponding author: shangdg@bjut.edu.cn

2 Experimental

2.1 Material

The chemical composition of the Ni-based superalloy GH4169 used in this investigation is listed in Table 1. The material was subjected to a heat-treatment condition from reference [19], including solid solution at 970°C for 1h, air cooling to 720°C, first-stage aging at 720°C for 8 h, furnace cooling at cooling rate of 50°C/h to 620°C, second-stage aging at 620 °C for 8 h, and air cooling to room temperature.

Table 1. Chemical composition of superalloy GH4169 (wt %).

C	0.07
Cr	20.00
Ni	53.00
Co	0.70
Mo	3.00
Al	0.50
Ti	1.00
Nb	5.10
B	0.01
Mg	0.01
Mn	0.30
Si	0.32
P	0.01
S	0.01
Cu	0.28
Ca	0.01
Pb	0.00
Fe	Balance

2.2 Axial-torsional thermo-mechanical fatigue testing

Thin-walled tubular specimen, with the gauge section thickness of 1mm, was adopted in all AT-TMF tests, as shown in Fig. 1. All tests were carried out on a tension-torsion closed-loop servo-hydraulic testing machine, which utilizes radio-frequency induction heating unit and forced air cooling pipe allowing rapid heating and cooling, as shown in Fig. 2. A high temperature tension-torsion extensometer with the gauge length of 25mm was used to measure the strains. A chromel-alumel (type K) thermocouple was used to measure the temperature on the middle outer surface of the gauge section.

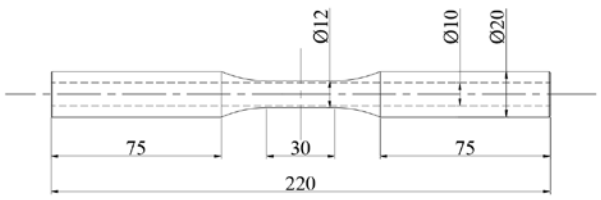

Fig. 1. Specimen geometry adopted in all AT-TMF tests.

Table 2. Loading conditions of AT-TMF tests.

Loading path	Loading waveform	Strain path
MIPTIP: Mechanical In-Phase, Thermal In-Phase	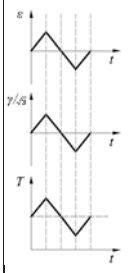	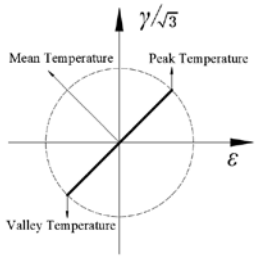
MIPTOP^{90}: Mechanical In-Phase, Thermal 90° Out-of-Phase	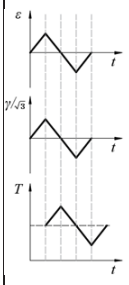	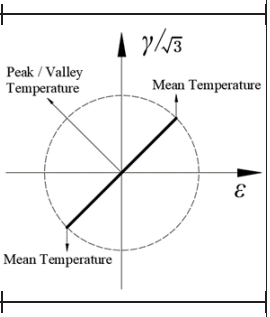
MIPTOP^{180}: Mechanical In-Phase, Thermal 180° Out-of-Phase	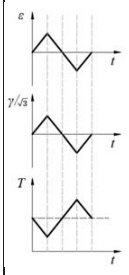	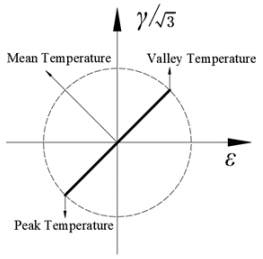
MOPTIP: Mechanical 90° Out-of-Phase, Thermal In-Phase	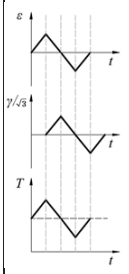	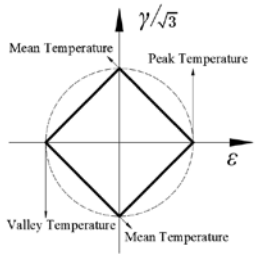
MOPTOP^{90}: Mechanical 90° Out-of-Phase, Thermal 90° Out-of-Phase	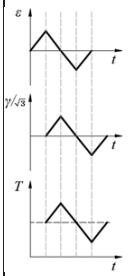	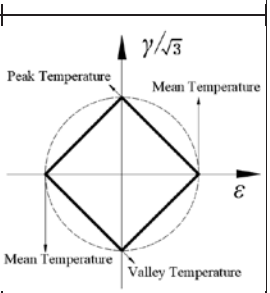
MOPTOP^{180}: Mechanical 90° Out-of-Phase, Thermal 180° Out-of-Phase	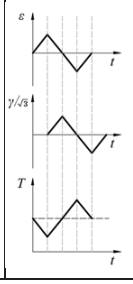	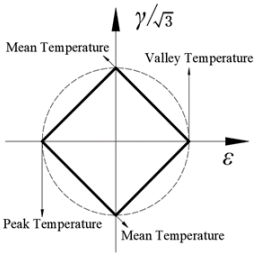

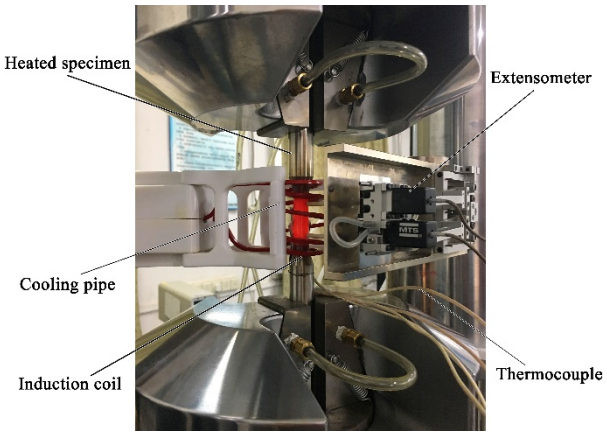

Fig. 2. Heated specimen, induction coil, cooling pipe, thermocouple and extensometer on the tension-torsion testing machine.

In AT-TMF tests, the axial thermal strain compensation was used [14], in which the axial total strain was calculated by adding the thermal strain to the mechanical strain ($\varepsilon_t = \varepsilon_m + \varepsilon_{th}$). For the torsional case, the shear strain is not influenced by the change of loading temperature [20], thus the torsional thermal strain compensation is not needed. Moreover, the equivalent mechanical strain (ε_{eq}) and the equivalent stress (σ_{eq}) at time t were calculated using the von Mises criterion [21]:

$$\varepsilon_{eq}(t) = \sqrt{[\varepsilon_m(t)]^2 + [\gamma(t)]^2/3} \quad (1)$$

where ε_m and γ are the axial mechanical strain and the shear strain, respectively.

$$\sigma_{eq}(t) = \sqrt{[\sigma(t)]^2 + 3[\tau(t)]^2} \quad (2)$$

where σ and τ are the axial stress and the shear stress, respectively. In addition, the thermal and mechanical phase angles both needed to be controlled for AT-TMF tests, and six different loading conditions were used in this investigation, as listed in Table 2.

The experimental parameters of AT-TMF tests are listed in Table 3. On the basis of the previous investigation [22], the non-proportional hardening was found to be obvious at the equivalent mechanical strain amplitude of 0.8%. For the purpose of effectively investigating the influence of non-proportional hardening on fatigue damage behavior under AT-TMF loading, the equivalent mechanical strain amplitude of all tests were selected at 0.8%. The ratios of mechanical shear and axial strains were 1.73 ($\sqrt{3}$) and 3.46 ($2\sqrt{3}$), which can be used to investigate the influence of strain ration on the fatigue damage behavior. Moreover, the tests were carried out in the temperature range from 360°C to 650°C. The cyclic period was 120s, and the loading frequency was about 0.0083Hz. The heating/cooling rate was calculated at about 4.83°C/s, which can maintain temperature uniformity in the gauge section of the specimen.

In addition, two thermal cycles with the mechanical loading of zero were implemented before the AT-TMF tests. The cyclic number corresponded to the decrease of 30% for stable peak stress was adopted as the fatigue failure life (N_f). After completing all tests, the scanning electron microscopy (SEM) was used to observe the morphology of fracture, and the energy dispersive x-ray analysis (EDAX) was employed to analyze the composition of fracture.

3 Experimental results and discussion

3.1 Varied fatigue lives under AT-TMF loading

Fig. 3 clearly shows that the fatigue lives are varied under AT-TMF loading even with the same equivalent mechanical strain amplitude of 0.8%. Moreover, thermal and mechanical phase angles have important influence on fatigue lives. The fatigue life is decreased when thermal phase angle is in-phase, and it is further reduced when mechanical phase angle is out-of-phase. As a result, the fatigue life under MOPTIP loading is the lowest. Furthermore, the fatigue life is relatively high under thermal 90° out-of-phase loading when the mechanical phase angle is the same, that is, MIPTOP^{90} > MIPTOP^{180} > MIPTIP, and MOPTOP^{90} > MOPTOP^{180} > MOPTIP, which means that the damage mechanisms are varied in different thermal phase cases. In addition, the strain ration also has important effect on fatigue lives. The fatigue life under MIPTIP loading with the strain ratio of 3.46 is higher than that with the strain ration of 1.73, which means that the fatigue damage behavior can be changed in different strain ratio cases. Therefore, it can be concluded that the varied damage mechanisms are the main reason of the obvious difference in fatigue lives under AT-TMF loading.

Table 3. Experimental parameters of AT-TMF tests.

Spec. no.	$\Delta\varepsilon_{eq}/2$ (%)	$\Delta\varepsilon_x/2$ (%)	$\Delta\gamma_{xy}/2$ (%)	Loading path	λ_ε	ΔT (°C)	t (s)
N1	0.800	0.566	0.980	MIPTIP	1.73	360-650	120
N2	0.800	0.566	0.980	MIPTOP^{90}	1.73	360-650	120
N3	0.800	0.566	0.980	MIPTOP^{180}	1.73	360-650	120
N4	0.800	0.800	1.386	MOPTIP	1.73	360-650	120
N5	0.800	0.800	1.386	MOPTOP^{90}	1.73	360-650	120
N6	0.800	0.800	1.386	MOPTOP^{180}	1.73	360-650	120
N7	0.800	0.358	1.239	MIPTIP	3.46	360-650	120

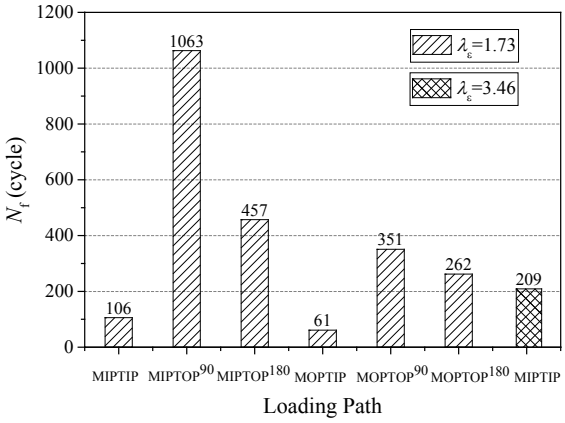

Fig. 3. Varied fatigue lives under AT-TMF loading ($\Delta\varepsilon_{eq}/2$=0.8%, ΔT=360°C-650°C, f=0.0083Hz).

3.2 Non-proportional hardening and mean stress under AT-TMF loading

Fig. 4 shows that the equivalent peak stress under MOPTOP^{90} loading is obviously higher than that under MIPTOP^{90} loading except the initial few cycles, which means that the non-proportional hardening can be induced in mechanical out-of-phase case. The non-proportional hardening can cause the enlargement of responded stress, which can increase the damage during fatigue loading process. It can be the main reason of that the fatigue lives under mechanical out-of-phase loading are lower than that under in-phase loading in the same thermal phase angle cases, that is, MOPTIP < MIPTIP, MOPTOP^{90} < MIPTOP^{90}, and MOPTOP^{180} < MIPTOP^{180}, as shown in Fig.3.

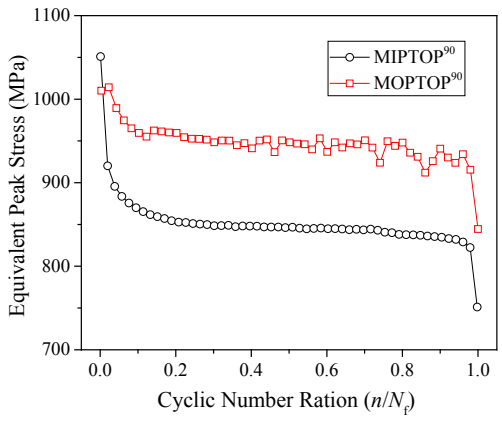

Fig. 4. Non-proportional hardening under AT-TMF loading ($\Delta\varepsilon_{eq}/2$=0.8%, λ_ε=1.73, ΔT=360°C-650°C, f=0.0083Hz).

Fig. 5 shows the special hysteresis loops under non-isothermal loading. The mean stress is induced when the peak and valley strain loadings correspond the different temperature points, that is, the negative mean axial stress under MOPTIP loading, and the positive mean axial stress under MOPTOP^{180} loading, as shown in Fig. 5 (a). And the mean stress is almost equal to zero when the peak and valley strain loadings correspond the same temperature point, as shown in Fig. 5 (b). It can be attributed to the dependence of responded stress on temperature. Moreover, the special deformation behavior under non-isothermal loading can induce the mean stress, which can influence the fatigue damage behavior.

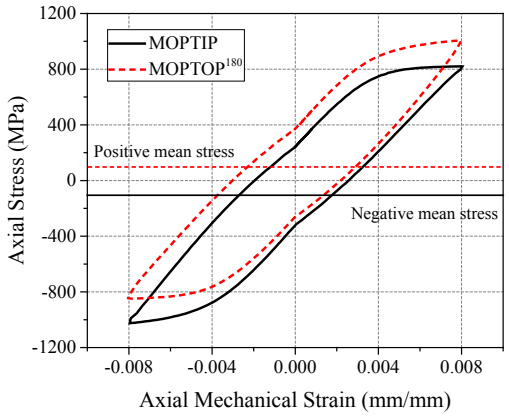

(a)

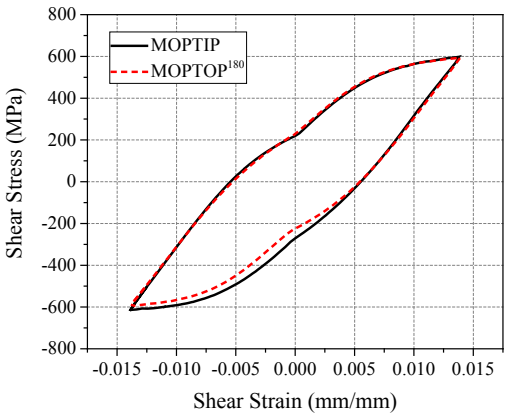

(b)

Fig. 5. Comparison of hysteresis loops under MOPTIP and MOPTOP^{180} loadings ($\Delta\varepsilon_{eq}/2$=0.8%, λ_ε=1.73, ΔT=360°C-650°C, f=0.0083Hz). (a) Axial hysteresis loop; (b)Torsional hysteresis loop.

3.3 Creep damage under AT-TMF loading

Fig. 6 shows that the dominant fracture mechanism is varied for different thermal phase angles even with the same mechanical phase angle. Fig 6 (a) and (c) show the visible morphology of grain boundaries, which means that the intergranular fracture is dominant under MIPTIP and MOPTIP loadings. The intergranular fracture implies that the creep damage is induced besides the fatigue damage, and it can be the main reason of the drastic decrease in fatigue life under thermal in-phase loading. However, the fatigue striation is evident in Fig.

6 (b) and (d), which means that the transgranular fracture is dominant under MIPTOP^{180} and MOPTOP^{180} loadings.

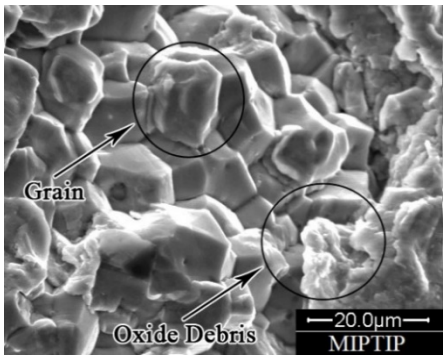

(a)

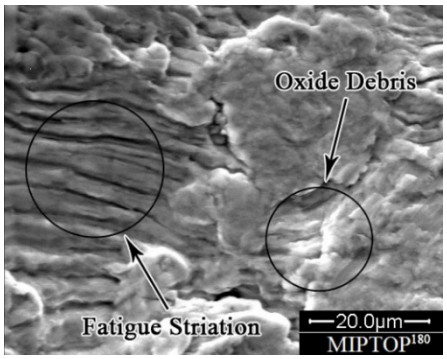

(b)

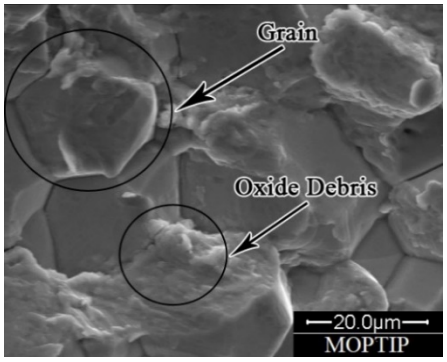

(c)

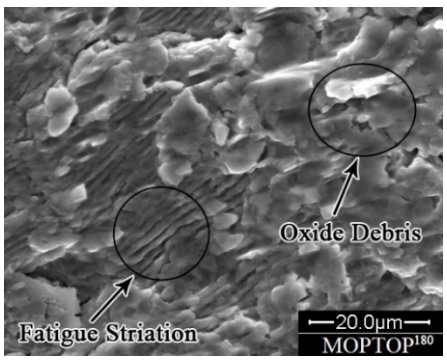

(d)

Fig. 6. Morphology of fracture under AT-TMF loading ($\Delta\varepsilon_{eq}/2$=0.8%, λ_ε=1.73, ΔT=360°C-650°C, f=0.0083Hz).
(a) Intergranular fracture under MIPTIP loading;
(b) Transgranular fracture under MIPTOP^{180} loading;
(c) Intergranular fracture under MOPTIP loading;
(d) Transgranular fracture under MOPTOP^{180} loading.

Thus it can be deduced that the creep damage is ignored, and the fatigue damage plays an important role in thermal out-of-phase loading. In conclusion, the creep damage is induced during thermal in-phase loading, which can cause the intergranular fracture, and the intergranular fracture can drastically decrease the fatigue life.

Fig. 7 (a) shows that the maximum tensile stress appears accompanied by the maximum temperature under MIPTIP loading. The creep damage can be induced by the tensile stress at high temperature, which is verified in the investigations concerning uniaxial TMF damage behavior [1-5]. Moreover, the creep damage can be further increased by the shear stress, since the shear stress can tear the creep cavities during cyclic loading. However, the maximum compressive stress appears when the shear stress and temperature reach their minimum values. The creep cavities cannot be sintered by the compressive stress due to the lower temperature [2]. Thus the creep cavities continuously grow and join during MIPTIP loading, and the intergranular fracture can be caused, which can be proved by the observed fracture mode in Fig. 6 (a).

Fig. 7 (b) shows that the tensile and shear stresses reach their maximum values when the temperature drops to its minimum value, and the maximum value of the temperature appears accompanied by the minimum values of compressive and shear stresses under MIPTOP^{180} loading. The creep damage cannot be induced in this condition, and the fatigue damage is dominant, which can be proved by the fracture feature in Fig. 6 (b).

Therefore, it can be concluded that the creep damage is induced by the tensile stress at high temperature, and it is increased by the shear stress during fatigue loading. It can be the main reason of that the fatigue life is decreased when thermal phase angle is in-phase, as shown in Fig. 3.

Moreover, the peak tensile stress under MIPTIP loading with the strain ration of 3.46 in Fig. 7 (c) is lower than that with the strain ratio of 1.73 in Fig. 7 (a). And the fatigue life under MIPTIP loading with strain ration of 3.46 is obviously higher than that with the strain ratio of 1.73, as shown in Fig. 3. Thus it can be deduced that the creep damage is lower at the strain ration of 3.46, and the decrease of tensile stress delays the nucleation of creep cavities at high temperature. However, the peak shear stress under MIPTIP loading with the strain ration of 3.46 in Fig. 7 (c) is higher than that with the strain ratio of 1.73 in Fig. 7 (a). Thus it can be deduced that the shear stress has a little influence on the nucleation of creep cavities at high temperature. In conclusion, the tensile stress has a significant influence on the nucleation of creep cavities at high temperature compared with the shear stress.

In addition, the extent of the creep damage depends on the magnitude of the stress and the temperature condition, and the non-proportional hardening can enlarge the responded stress, as show in Fig. 4. Thus it

can be deduced that the non-proportional hardening can increase the creep damage, which can be a main reason of that the fatigue life under MOPTIP loading is obviously lower than that under MIPTIP loading, as shown in Fig. 3.

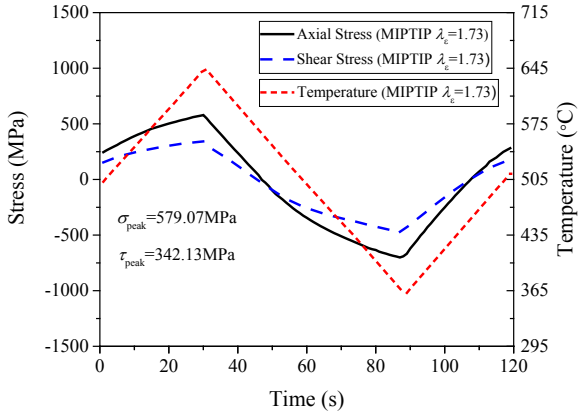

(a)

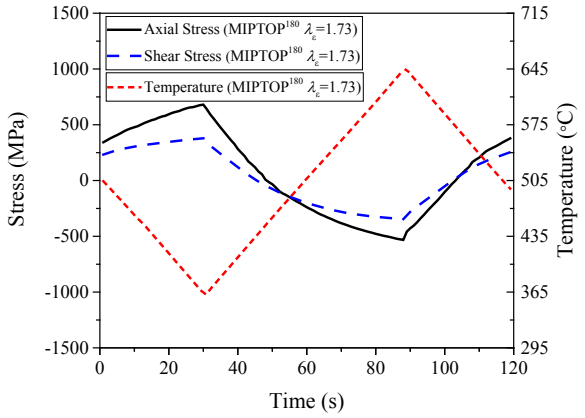

(b)

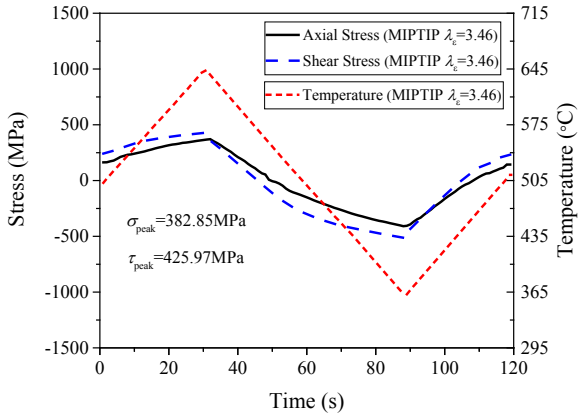

(c)

Fig. 7. Responded axial and shear stresses with temperature under AT-TMF loading ($\Delta\varepsilon_{eq}/2$=0.8%, ΔT=360°C-650°C, f=0.0083Hz). (a) MIPTIP, λ_ε=1.73; (b) MIPTOP^{180}, λ_ε=1.73; (c) MIPTIP, λ_ε=3.46.

3.4 Oxidation damage under AT-TMF loading

Fig. 6 also shows the oxide debris in all loading conditions, and the existence of the oxide debris can be proved by the appeared oxygen atom in the chemical composition of the fracture, as shown in Fig. 8. The observed oxide debris implies that the oxidation damage can be induced during fatigue loading at elevated temperature. Furthermore, the oxygen content is changed, which can express the varied degree of oxidation damage in different loading conditions. Compared with the mechanical in-phase loading, the oxidation is more serious under mechanical out-of-phase loading, that is, for oxygen content MOPTIP > MIPTIP, and MOPTOP^{180} > MIPTOP^{180}. And the oxidation damage is more serious under thermal 180° out-of-phase loading than that under thermal in-phase loading, that is, for oxygen content MIPTOP^{180} > MIPTIP, and MOPTOP^{180} > MOPTIP. Therefore, it can be concluded that the oxidation damage is varied with the different thermal and mechanical phase angles under AT-TMF loading.

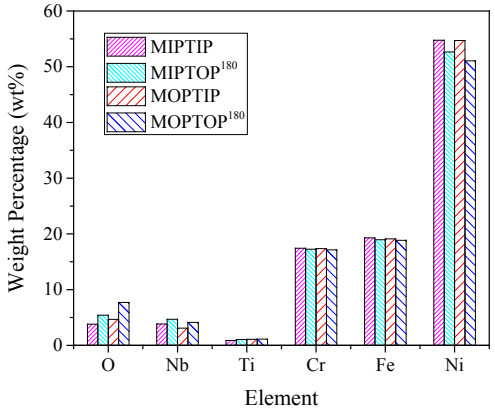

Fig. 8. Chemical composition of fracture under AT-TMF loading ($\Delta\varepsilon_{eq}/2$=0.8%, λ_ε=1.73, ΔT=360°C-650°C, f=0.0083Hz).

The extent of the oxidation damage also depends on the magnitude of stress and the temperature condition [23]. It can be deduced that the non-proportional hardening can increase the oxidation damage. As a result, the oxygen content under mechanical out-of-phase loading is higher than that under in-phase loading, as shown in Fig. 8. Furthermore, the increase of oxidation damage from non-proportional hardening can be a important reason of that the fatigue life is reduced when mechanical phase angle is out-of-phase, as shown in Fig. 3.

Moreover, the oxidation damage can be increased by the tensile mean stress induced during non-isothermal loading, which is verified in the investigations [9-12]. It can be the main reason of that the oxygen content under thermal 180° out-of-phase loading is higher than that under in-phase loading, as shown in Fig. 8.

In addition, the temperature corresponding the peak/vallley strain loading under thermal 90° out-of-

phase loading (505°C) is lower than the temperature corresponding the valley strain loading under thermal 180° out-of-phase loading (650°C) in mechanical in-phase loading case. It can be deduced that the oxidation damage is lower under thermal 90° out-of-phase loading. As a result, for the fatigue life $MIPTOP^{90} > MIPTOP^{180}$, and $MOPTOP^{90} > MOPTOP^{180}$, as shown in Fig. 3.

Therefore, it can be concluded that the oxidation damage is induced during fatigue loading at high temperature. Moreover, the oxidation damage can be increased by the non-proportional hardening from mechanical out-of-phase loading and the tensile mean stress induced during non-isothermal loading.

4 Conclusions

The fatigue damage behavior was experimentally investigated for Ni-based superalloy under different AT-TMF loading conditions with the same equivalent mechanical strain amplitude. Some key conclusions are obtained as follows:

(1) The fatigue life is drastically decreased when the axial mechanical strain and the temperature are in-phase, which can be attributed to that the creep damage is induced by the tensile stress at high temperature.

(2) The fatigue life is further reduced when the axial mechanical strain and the shear strain are out-of-phase, since the non-proportional hardening can increase the creep and the oxidation damages.

(3) The tensile stress has an important effect on the nucleation of creep cavities at high temperature compared with the shear stress. However, the tensile and shear stresses both can increase the creep damage under cyclic loading at high temperature.

(4) The oxidation damage can be induced during fatigue loading at high temperature, and it can be increased by the tensile mean stress caused in non-isothermal loading.

The authors gratefully acknowledge the financial support of the National Natural Science Foundation of China (No. 51535001, 11572008).

References

1. A.G.D.L. Yedra, J.L. Pedrejón, A. Martín-Meizoso, R. Rodríguez, Exp. Techniques **40**, 777-787 (2014)
2. S. Guth, S. Doll, K.H. Lang, Mater. Sci. Eng. A **642**, 42-48 (2015)
3. G.V.P. Reddy, A. Nagesha, R. Sandhya, S. Sankaran, M.D. Mathew, K.B.S. Rao, Metall. Mater. Trans. A **46**, 695-707 (2015)
4. D. Lee, I. Shin, Y. Kim, J.M. Koo, C.S. Seok, Int. J. Fatigue **62**, 62-66 (2014)
5. Z.W. Huang, Z.G. Wang, S.J. Zhu, F.H. Yuan, F.G. Wang, Mater. Sci. Eng. A **432**, 308-316 (2006)
6. R. Petráš, V. Škorík, J. Polák, Mater. Sci. Eng. A **650**, 52-62 (2016)
7. S. Guth, R. Petráš, V. Škorík, T. Kruml, J. Man, K.H. Lang, J. Polák, Int. J. Fatigue **80**, 426-433 (2015)
8. X. Hu, D. Shi, X. Yang, Mater. Sci. Eng. A **674**, 451-458 (2016)
9. K. Prasad, C. Parlikar, D.K. Das, Int. J. Fatigue **92**, 107-115 (2016)
10. K. Prasad, R. Sarkar, K.B.S. Rao, M. Sundararaman, Metall. Mater. Trans. A **47A**, 1-18 (2016)
11. P. Schallow, H.J. Christ, Int. J. Fatigue **53**, 15-25 (2013)
12. A. Nagesha, R. Kannan, V.S. Srinivasan, R. Sandhya, B.K. Choudhary, K. Laha, Metall. Mater. Trans. A **47**, 1-18 (2016)
13. P.J. Bonacuse, S. Kalluri, AGARD CP **569**, 15 (1996)
14. S. Kalluri, P.J. Bonacuse, ASTM STP **1280**, 184-207 (1997)
15. J. Meersmann, F. Frenz, J. Ziebs, H.J. Kuhn, S. Forest, AGARD CP **569**, 19 (1996)
16. S.P. Brookes, H.J. Kühn, B. Skrotzki, H. Klingelhöffer, R. Sievert, J. Pfetzing, D. Peter, G. Eggeler, Mater. Sci. Eng. A **527**, 3829-3839 (2010)
17. A. Gosar, M. Nagode, Int. J. Fatigue **48**, 223-230 (2013)
18. P. Wang, L. Cui, A. Scholz, S. Linn, M. Oechsner, Int. J. Fatigue **67**, 220-227 (2014)
19. Editorial Committee of China Aeronautical Materials Handbook, China Aeronautical Materials Handbook **2nd ed.**, (2002)
20. C.E. Bakis, M.G. Castelli, J.R. Ellis, ASTM STP **1191**, 223-243 (1993)
21. X.W. Wang, D.G. Shang, Int. J. Fatigue **90**, 36-46 (2016)
22. D.G. Shang, G.Q. Sun, J.H. Chen, N. Cai, C.L. Yan, Mater. Sci. Eng. A **432**, 231-238 (2006)
23. F. Vöse, M. Becker, A. Fischersworring-Bunk, H.P. Hackenberg, Int. J. Fatigue **53**, 49-57 (2013)